Depth of Laser Etching in Green State LTCC

Krzysztof Zaraska*, Monika Machnik, Adam Bieńkowski, Beata Synkiewicz
Institute of Electron Technology Kraków Division, ul. Zabłocie 39, 30-701 Kraków, Poland
** Phone: +48126563144 ext. 254, Fax: +48126563626, kzaraska@ite.waw.pl*

Abstract

Laser etching of green state LTCC is a useful rapid prototyping and precision manufacturing process. Laser etching allows selective removal of screen printed conductor layer, producing patterns with higher precision than conventional screen printing. Its usefulness for rapid prototyping is due to elimination of time consuming screen preparation process. The etching is performed using a near UV (355 nm), pulsed laser. The process is characterized by three parameters: laser power, pulse frequency, and etching speed. From the practical standpoint, we are interested in finding a combination of parameters which allows for achieving required etching depth at the maximum etching speed. We present an empirical mathematical model relating etching depth to process parameters, allowing to theoretically determine optimum processing parameters for a specified etching depth.

Keywords: LTCC, laser, modeling

1 Introduction

We investigate application of laser etching for producing precise conductor patterns in the LTCC process. This technology has been used before in order to produce heaters [2], gas sensors [1], and microwave circuits [5].

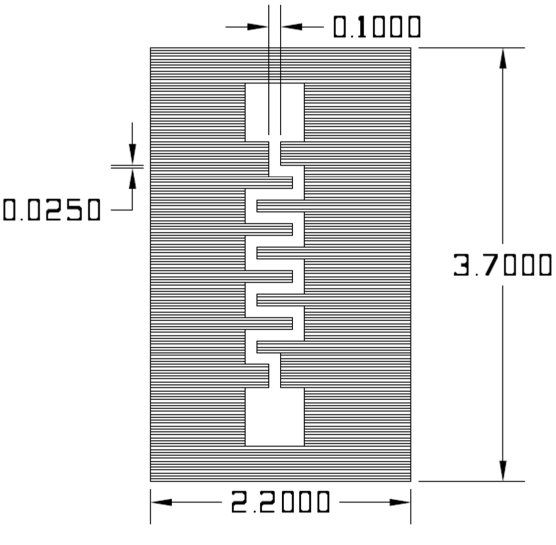

Fig. 1. Machining drawing of a microwave inductor to be produced by laser etching method. Dimensions in mm.

We start with a green state LTCC sheet with a uniform conductor layer printed on top. In this investigation, we have used DP951 tape and DP6142D Ag conductor composition. The thickness of the printed layer is about 20µm. Then, we use a pulsed Nd:YAG laser (355nm, 10W) to selectively remove the conductor material. Material removal is performed by machining a series of parallel lines covering the removal area. (Fig. 1). The lines are spaced every 25 µm, which corresponds to twice the laser beam width on the substrate (10 µm).

The method is useful for producing fine patterns (resulting line precision is about 5 µm) [1]. It is also extremely useful for rapid prototyping, as the screen preparation process is eliminated. Instead, tapes with standard conductor patterns are printed in advance, stored, and then machined into requested pattern as necessary.

An unintended side effect of this method is that, besides the desired removal of the conductor layer, removal of substrate material occurs. This effect is undesirable, and should be minimized; the simplest reason is that excess removal of substrate material weakens the structure mechanically, and can contribute to substrate bending during firing. Related surface properties of laser-processed LTCC have been described before [6].

In this study, following our earlier work on the subject [7], we have attempted to perform a systematic investigation of laser ablation depth in green-state LTCC, in function of processing parameters. Implications of this work go beyond using laser for etching conductor paths. Determining relationship between machining parameters and resulting cut depth is also valuable for more common tasks in LTCC processing, such as cutting sheets and via holes. Here, results of our investigation can be used in order to optimize the processing speed and increase precision. This paper takes a purely empirical approach, without considering underlying physical mechanisms of interaction between laser light and processed material. For more information on the subject, see e.g. [3].

On our laser system, the following parameters can be controlled:

- Output laser power is set by attenuating the beam through a set of polarizing filters. The laser source thus works at a constant power, and the filter is used to adjust the power of the output beam. Hereinafter, the variable *p* refers to attenuator setting, between 0% (fully closed) and 100% (fully open).
- Laser pulse frequency *f*, i.e. number of laser pulses generated per second. It must be noted, that the laser system in question exhibits a non-trivial relationship between operation frequency and output power (Fig. 2).
- Machining speed, or feedrate, *v* (in mm/s) describes speed of movement of the laser beam on the processed substrate.

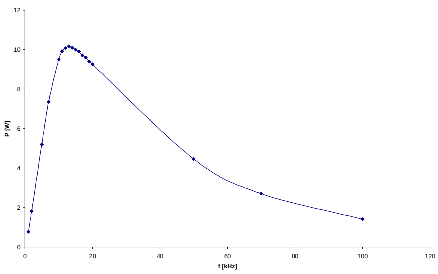

Fig. 2. Equivalent DC power of the laser source, in function of operation frequency.

2 Experimental data

Mathematically speaking, we can consider a function *d(p,f,v)* representing ablation depth in function of processing parameters. Three input parameters mean that we must search a three-dimensional parameter space. For example, if we want to investigate 10 different values for each input parameter, then we must perform 10^3 = 1000 tries. We have thus performed machining for 4 values of each parameter, forming a 4x4x4 grid. This grid will be used for model fitting. This grid is complemented by a second 4x4x4 grid, which will be used for validating the fitted model. The points of secondary grid are chosen to lie in between the points of the primary grid (Fig. 3). We thus have to perform only 2x4x4x4=128 experiments.

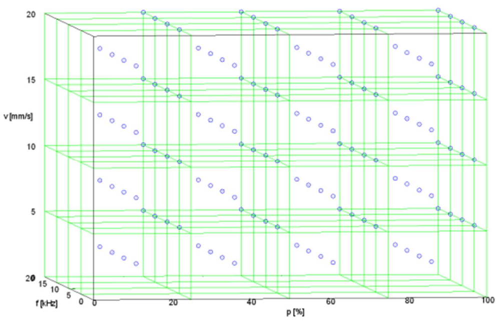

Fig. 3. Primary (fitting) and secondary (validation) data grids. Measurement points are marked with blue circles. Points which lie on the intersection of green lines form the primary grid.

The experimental protocol was as follows. Sheets of DP951 tape (200µm thickness) have been laminated together. On the top layer, a 20µm thick layer of DP6142D conductor has been deposited using standard screen-printing process. On each stack, a series of single-pass laser cuts has been performed with different processing parameters (see Table 1 & 2). Then, cross-sections of laser cuts have been obtained by cutting the layer stack mechanically in the direction perpendicular to the direction of the laser cut. Hirox KH-7700 optical microscope has been used to photograph the cross-sections and measure depth of the laser-produced trench.

The experimental data is summarized in Table 1 and 2. We observe that both material etching and cutting can be performed by varying the processing parameters appropriately (Fig. 4). We further observe, that the relationship between ablation depth and input parameters is non-linear.

Comparison of data obtained for processing just the green tape material (Table 1) and green tape material with printed conductor layer (Table 2) shows, that presence of conductor paste on the surface changes the behavior of the material (see Fig. 5). However, no simple relationship between the behavior of unprinted and printed tape can be derived. From a practical standpoint, it is thus better to treat the tape with printed conductor as a different material.

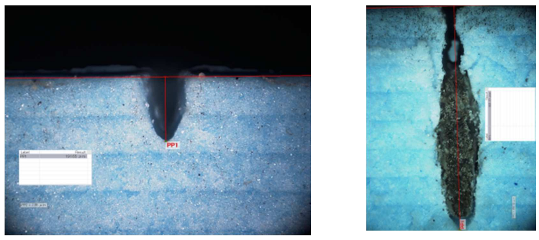

(a) (b)

Fig. 4. Example cross-sections of laser cuts for different processing parameters. (a) *f*=5 kHz, *v*=5mm/s, *p*=75%, *d*=433µm (b) *f*=10 kHz, *v*=5mm/s, *p*=100%, *d*=901µm

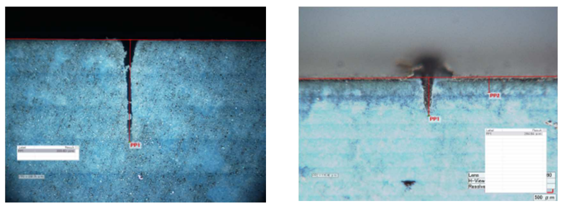

(a) (b)

Fig. 5. Comparison of cross-sections of green tape without (a) and with (b) a conductor layer, for the same processing parameters: *f*=20 kHz, *v*=20mm/s, *p*=75%. Also note difference in geometry of the cut.

Table 1a. Experimental ablation depth (µm) for LTCC material. Primary grid.

	v=5mm/s				v=10mm/s			
p\f	5 kHz	10 kHz	15 kHz	20 kHz	5 kHz	10 kHz	15 kHz	20 kHz
25%	240.43	331.99	295.47	266.55	128.47	314.91	291.14	284.26
50%	304.80	637.60	530.94	479.27	252.94	353.91	425.78	415.20
75%	433.80	797.84	694.56	765.95	316.45	445.17	543.76	526.33
100%	400.29	901.17	853.39	800.57	320.53	541.32	646.64	573.93
	v=15mm/s				v=20mm/s			
p\f	5 kHz	10 kHz	15 kHz	20 kHz	5 kHz	10 kHz	15 kHz	20 kHz
25%	116.27	192.11	317.74	267.62	74.14	146.07	153.19	145.76
50%	204.44	298.52	312.22	295.35	119.80	229.53	250.86	236.06
75%	191.65	343.30	396.94	346.27	149.20	274.18	323.91	355.40
100%	234.74	403.87	480.94	450.17	174.64	320.42	366.60	382.93

Table 1b. Experimental ablation depth (µm) for LTCC material. Secondary grid.

	V=2.5mm/s				V=7.5mm/s			
p\f	2.5kHz	7.5kHz	12.5kHz	17.5kHz	2.5kHz	7.5kHz	12.5kHz	17.5kHz
12.50%	172.53	225.73	384.23	290.50	60.51	240.92	239.07	232.11
37.50%	277.92	742.67	736.13	723.67	160.74	373.02	473.38	459.56
62.50%	325.07	987.32	1108.06	919.42	270.09	458.17	580.41	694.98
87.50%	408.06	1208.04	1415.17	1203.35	307.98	623.09	696.09	778.33
	v=12.5mm/s				V=17.5mm/s			
p\f	2.5kHz	7.5kHz	12.5kHz	17.5kHz	2.5kHz	7.5kHz	12.5kHz	17.5kHz
12.50%	69.63	92.76	137.11	174.46	30.78	82.58	98.61	82.39
37.50%	120.89	263.16	341.44	297.96	58.69	149.26	198.42	201.28
62.50%	112.10	303.83	438.36	454.38	82.85	195.91	247.45	288.30
87.50%	148.77	419.87	527.88	547.75	91.33	225.81	309.67	412.86

Table 2a. Experimental ablation depth (µm) for LTCC material with conductor layer. Primary grid.

	v=5mm/s				v=10mm/s			
p\f	5 kHz	10 kHz	15 kHz	20 kHz	5 kHz	10 kHz	15 kHz	20 kHz
25%	250.11	429.44	317.08	349.19	128.17	271.20	367.77	191.84
50%	399.26	598.89	542.70	567.19	260.01	391.54	481.36	426.81
75%	475.02	697.15	684.96	676.20	330.06	496.78	585.33	551.99
100%	528.55	851.08	879.57	791.78	353.06	572.93	584.74	614.01
	v=15mm/s				v=20mm/s			
p\f	5 kHz	10 kHz	15 kHz	20 kHz	5 kHz	10 kHz	15 kHz	20 kHz
25%	73.80	184.63	310.76	203.21	126.87	182.40	203.92	111.36
50%	174.29	247.43	291.44	311.51	142.44	244.35	295.77	198.13
75%	225.84	267.68	365.38	405.73	174.12	295.58	368.55	284.84
100%	261.60	327.60	400.09	489.91	205.69	315.74	423.89	394.43

Table 2b. Experimental ablation depth (µm) for LTCC material with conductor layer. Secondary grid.

	v=2.5mm/s				v=7.5mm/s			
p\f	2.5kHz	7.5kHz	12.5kHz	17.5kHz	2.5kHz	7.5kHz	12.5kHz	17.5kHz
12.50%	123.29	298.34	347.54	354.78	60.00	127.33	261.71	239.35
37.50%	347.24	770.62	726.33	693.15	162.75	394.89	482.31	343.60
62.50%	398.22	906.77	988.57	845.30	217.07	462.52	641.05	574.56
87.50%	461.15	1047.57	1140.00	971.60	247.22	537.16	780.00	708.59
	v=12.5mm/s				v=17.5mm/s			
p\f	2.5kHz	7.5kHz	12.5kHz	17.5kHz	2.5kHz	7.5kHz	12.5kHz	17.5kHz
12.50%	33.57	216.57	231.60	176.73	27.60	124.96	135.94	182.54
37.50%	72.99	267.47	350.37	334.96	56.57	224.00	220.28	238.73
62.50%	116.27	318.20	360.53	418.91	129.84	243.51	259.59	304.71
87.50%	193.50	400.41	480.61	466.36	167.94	261.35	283.23	336.06

Table 3. Summary of models.

Powers of v			Removed data		Polynomial degree		Constants			Weighted relative error [%]		Pearson corr. coeff.
i_1	i_2	i_3	p[%]	f[kHz]	for α	for β	for i_1	for i_2	for i_3	Validation set	Testing set	
2	1	0	25	20	2	2	0.00	-0.15	6.62	23.71	40.41	0.86
1	0	-1	100	0	2	2	-0.05	6.39	-0.54	24.12	29.55	0.98
2	1	0	25	0	1	3	0.00	-0.06	6.74	25.62	39.45	0.77
2	1	0	25	0	2	2	0.00	-0.09	6.74	27.20	32.20	0.95

As far as minimizing substrate disruption during the conductor removal is concerned, data from Table 2 tell us that the best parameter set is *p*=12.5%, *f*=2.5kHz, *v*=17.5mm/s. This results in the ablation depth of 27.6µm, just a few micrometers more than the thickness of the conductive layer itself. It is also worth noting that we have not been able to determine a parameter set which would fail to remove the conductor.

3 Modeling

Because of complex relationship between processing parameters and resulting ablation depth, we attempt to create a mathematical model, approximating the resulting ablation depth for specified processing parameters *(p,f,v)*. Armed with such model, we can answer the following question: how to set processing parameters in order to obtain desired ablation depth. Due to the primary application being related to using laser etching to form conductive patterns, the modeling has been done for the case of substrate covered with the conductive layer (data from Table 2).

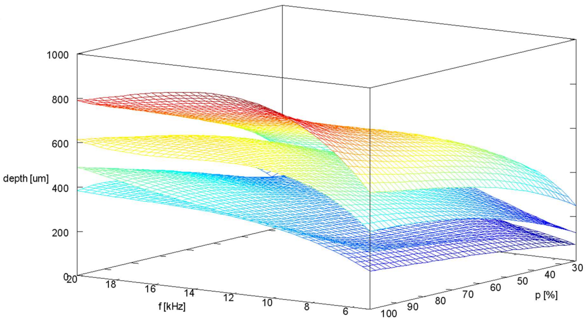

Fig.6. Surfaces representing ablation depth (in micrometers) depending on laser power (*p*) and frequency (*f*) (experimental data, spline interpolation). The drawn surfaces correspond to different machining speeds, from top to bottom: *v*=5,10,15,20 mm/s.

Multivariate data analysis becomes more problematic as dimensionality increases. For that reason, we have analyzed all functions of depth dependent on one variable and note quasi-exponential relationship to the beam speed. Due to that dependency of a depth d with an speed v, the model can be in general expressed by the equation:

$$d(p,f,v) = \exp\left(\prod_{i \in I} S_i(p,f) \cdot v^i\right),$$

where: S_i is some unknown function of two variables and I is 3-element subset of integers and $0 \in I$. The tests show that I equals to $\{2,1,0\}$ or $\{1,0,-1\}$ is sufficient.

Monocity study of the depth function leads us to the following results: increasing beam power increases depth, and so does decreasing speed. Dependency on frequency is not obvious and hence omitted. However, the experimental data do not comply with that in some regions of the domain (mainly for $p = 25\%$). This situation could be caused by additional effects like absorbing the energy of the beam by silver or partial melting. As a conclusion, modeling procedure takes into consideration throwing out some approximation data only if doing so reduces the error rate on validation set. In that case the validation set must be also restricted, due to big error rate of extrapolation. Table 4 lists in rows values which could be removed from both sets.

Table 4. Datapoints that could be removed from approximation and validation sets.

approximation set		validation set	
p[%]	f[kHz]	p[%]	f[kHz]
100	0	87,5	0
25	0	12,5	0
0	20	0	17,5

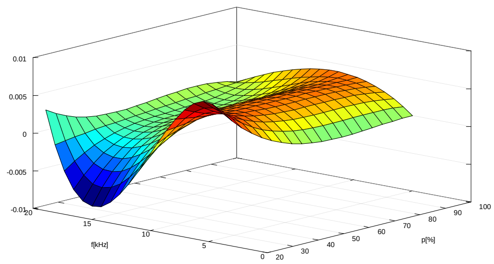

(a)

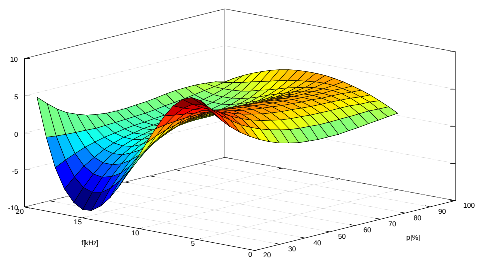

(b)

Fig. 7. Graphs of functions shows S_2 with $I = \{2,1,0\}$ (a) and S_{-1} with $I = \{1,0,-1\}$ (b).

In the next step we interpolate planes S_i with splines in order to describe them further. Fig. 7 shows S_2 where $I = \{2,1,0\}$ (a) and S_{-1} where $I = \{1,0,-1\}$ (b) act similar (and so do the other planes), and for every plane S_i fibers with constant p are similar to a scale and a translation, thus we can apply to them the same model expressed by the equation:

$$S(p,f) = \alpha(p) \cdot \prod_{j=1}^{3}\left(f - \beta_j(p)\right) + c, (*)$$

where: α is a polynomial of degree 1 or 2, β_j $(j = 1,2,3)$ is a polynomial of degree 2 or 3, and c is a constant. Above formula is a result of the reasoning given below.

For every fiber corresponding to $p = 25,50,75,100$ we approximate the created function F of variable f with polynomial of degree 3:

$$F_p(f) = a_p \cdot f^3 + b_p \cdot f^2 + c_p \cdot f^1 + d_p.$$

Since now we want to have an intercept form of this polynomial , we must ensure that the polynomial has three real roots. Basing on the well-known to properties of real polynomials, algorithm calculates the range for constant c. However, in some situations, numerical errors can cause that polynomial to have more roots than it is possible due to Fundamental Theorem of Algebra; that is also taken into consideration. When we have the proper range for the constant c for which the problem of complex roots is eliminated, we take a subset of five equidistant points from the range. At this point for every value of c from that subset, we can obtain an intercept form of above polynomial:

$$F_p(f) = a_p \cdot (f - f_{1,p}) \cdot (f - f_{2,p}) \cdot (f - f_{3,p}).$$

Next, we make approximation over second variable, that is p. By approximating a_p, $f_{1,p}$, $f_{2,p}$ and $f_{3,p}$ in points $p = 25,50,75,100$ with polynomials of proper degree we get $\alpha(p)$ and $\beta_j(p), j = 1,2,3$ in (*).

For every possible values of powers of v, degrees of polynomials α and β, constant c in every of the three planes, and four ways of discarding the potentially noisy data we calculate the mean relative error on validation data. Since we are more interested in depth values in points corresponding to bigger values of speed, the weight for each point is equal the value of coordinate v. We also note, that using polynomial of degree not higher than 3 helps to avoid Runge's phenomenon. By minimizing the errors we obtain the final model and test it. Since we cannot use the same data for training the model and for testing it, we split the secondary grid data into two sets: the validation set which is used for training the model, and the test set which is used for testing the trained model.

4 RESULTS

The summary of models is given in table 3. The model given in row 2 represents the best fit, and we analyze it further. Fig. 8 shows relative approximate errors in the points of the secondary grid. For comparison, Fig. 9 shows the same errors calculated for the simple spline interpolation model.

By comparing Fig. 8 and 9 we observe, that our model suffers from smaller errors for low power settings than the spline model. Further, we observe lower errors for higher machining speed (v). This behavior has been induced on purpose, by appropriately manipulating the weights used in model training. The reason behind this is that we are more interested in high processing speeds – hence, we trade model's accuracy for a low v (which is not interesting) for an increased accuracy at higher v values. We further note, that our model is capable to offer prediction for the lowest machining speed v=2.5mm/s, (albeit with a large error), while a spline-based approach cannot be used to extrapolate outside the data grid. Overall however, our model suffers from worse accuracy than the splines method.

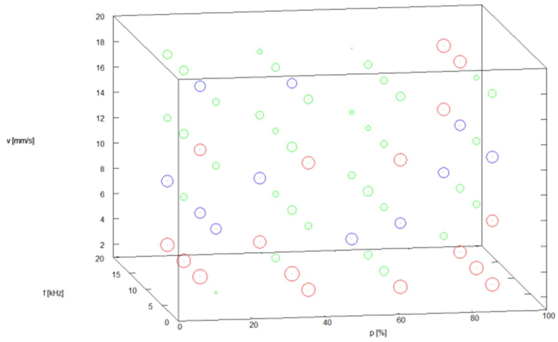

Fig. 8. Relative approximation errors for points in the secondary grid (our model). Green – below 12,5%, blue – below 25%, red – above 25%.

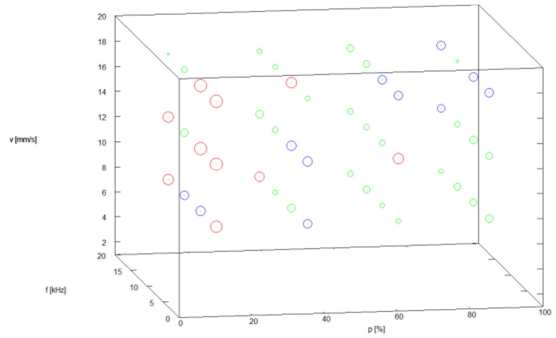

Fig. 9. Relative approximation errors for points in the secondary grid (spline method). Green – below 12,5%, blue – below 25%, red – above 25%.

Despite that we obtain a model that has the error rate bigger than the error rate of a standard spline method ($err_{spline} = 24{,}0\%$), its error rate is still acceptable ($err_{test} = 29{,}5\%$) and results still may be very useful. We point out that its main application is not to exactly predict the depth of laser cut, but to point values of p, f and v that gives the specified value of d. That means, we don't have to know all of the *(p,f,v)* points meeting our requirement, but only some of them. This kind of modeling can thus use weighted error during the training, to minimize error in the desired region of the domain. For obtaining better results, we can take the intersection of the results of both methods (i.e. the model method and the spline method).

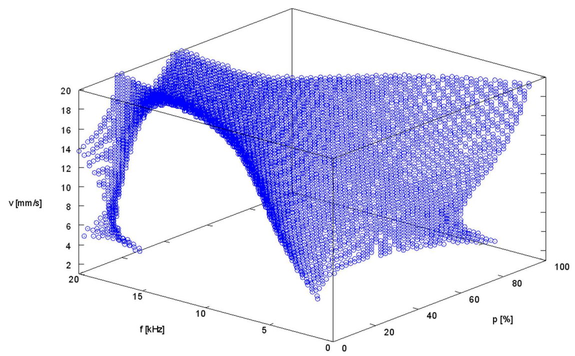

Fig. 10. Points representing all possible *(p,f,v)* triplets resulting in the ablation depth of 200±10 µm.

Fig. 10 graphically shows all combination of processing parameters, which will result in obtaining pre-determined ablation depth (*d*=200±10µm). We observe, that different ablation parameters can result in the same ablation depth. For this reason, we can choose processing parameters to use based on other considerations, such as maximum processing speed (i.e. highest possible value of feedrate *v*). Fig. 11 shows all possible *(f,p)* pairs, resulting in ablation depth *d*=200±10µm at feedrates between 19.5 and 20 mm/s.

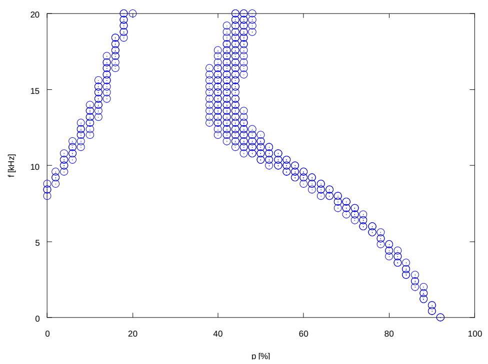

Fig. 11. Possible combinations of laser power (*p*) and frequency (*f*), resulting in ablation depth of 200±10 µm at feedrates between 19.5 and 20 mm/s.

5 Conclusions

We have succeeded in experimentally determining approximate relationships between laser machining parameters: laser power, frequency and machining speed and resulting trench depth in an unfired LTCC green tape.

We observe that the presence of conductor material on the tape changes its behavior under laser processing.

We have been able to experimentally determine the parameter set which removes the conductor material, while minimizing destruction of the underlying substrate material.

The developed mathematical model allows us to predict resulting trench depth from processing parameters with less than 25% relative error in most cases. We also observe that the same ablation depth can be achieved by different combination of settings. Hence, processing settings for particular ablation depth can be chosen taking into account secondary objectives, such as processing speed.

This allows us to theoretically solve the inverse problem, i.e. determine optimal processing parameters for a specified trench depth. This eliminates a time-consuming trial-and-error process.

6 Bibliography

[1] Bieńkowski A., Gaudyn J., Zaraska K., Rydosz A., Maziarz W., Malecha K.: *Laser Micromachined LTCC Gas Sensors*, Elektronika, vol. LI, no. 3, pp. 90-92 (2011).

[2] Kita J., Dziedzic A., Golonka L.J., Bochenek, A. *Properties of laser cut LTCC heaters*, Microelectronics Reliability, Vol. 40 No. 6, pp. 1005-1010 (2000)

[3] Majumdar J. D., Manna I., *Laser Processing of Materials*, Sadhana vol. 28, pp. 495-562 (2003)

[4] Quarteroni A., Saleri F., Gervasio P. *Scientific computing with MATLAB and Octave*, Springer, 2010

[5] Shafique M.F., Steenson D.P., *Laser Prototyping of Microwave Circuits in LTCC Technology*, IEEE Trans. Microwave Theory and Techniques, Vol. 57 No. 12 (2009)

[6] Zaraska K., Gaudyn J., Bieńkowski A., Czerwiński A., Płuska M., *Surface Properties of Laser-Etched LTCC Ceramic*, Proc 44th International Symposium on Microelectronics, Long Beach, 2011, pp. 735-739.

[7] Zaraska K., Groeger B., Bieńkowski A., Guzdek P., Cież M., Zaraska W.: *Investigation of Machining Parameters for Laser Patterning of LTCC Conductive Layers*, Proc 33th International Conference and Exhibition IMAPS - Poland 2009, Gliwice-Pszczyna, 21-24 September 2009,pp. 367-370.